4968 *Macromolecules* **2010**, *43*, 4968–4977
DOI: 10.1021/ma100384j

Macromolecules
ARTICLE

Segmental and Normal Mode Relaxation of Poly(alkylene oxide)s Studied by Dielectric Spectroscopy and Rheology

Christine Gerstl,*,† Gerald J. Schneider,*,† Wim Pyckhout-Hintzen,† Jürgen Allgaier,† Dieter Richter,† Angel Alegría,‡ and Juan Colmenero§

†*Institut für Festkörperforschung, Neutronenstreuung, Forschungszentrum Jülich, 52425 Jülich, Germany,* ‡*Centro de Fisica de Materiales CSIC-UPV/EHU, Edificio Korta, 20018 San Sebastián, Spain, Departamento de Física de Materiales UPV/EHU, Facultad de Química, Apartado 1072, 20080 San Sebastián, Spain, and* §*Centro de Fisica de Materiales CSIC-UPV/EHU, Edificio Korta, 20018 San Sebastián, Spain, Departamento de Física de Materiales UPV/EHU, Facultad de Química, Apartado 1072, 20080 San Sebastián, Spain, Donostia International Physics Center, Paseo Manuel de Lardizabal 4, 20018 San Sebastián, Spain*

Received February 22, 2010; Revised Manuscript Received March 30, 2010

ABSTRACT: A series of poly(alkylene oxide)s (PAO's) with different lengths of the side chains and two different molecular weights were studied by means of differential scanning calorimetry, dielectric spectroscopy (BDS), and rheology. The glass transition temperatures are almost independent of molar mass and the length of the side chains, which is also reflected by the dielectric α-relaxation, which depends only slightly on the different samples. However, the corresponding maxima in the dielectric loss of the samples with longer side chains show a shoulder at high frequencies with a temperature-dependent shape. The shape of the normal mode changes slightly with the molar mass and the length of the side chain. The normal mode relaxation times show a molar-mass-dependent behavior indicating a significant increase of the entanglement molecular weight M_e with increasing length of the side group. A Rouse mode analysis incorporating the molar mass distribution was performed but could not reproduce the experimental data of the normal mode process completely. The relaxation times obtained by rheology agree well with the dielectric results, and estimates of M_e based on the number of entanglements and on the packing model confirm the values suggested by BDS. A comparison of the estimated chain dimensions with literature data supports the reliability of our calculations.

Introduction

Compared to polymers without side groups, a dramatic drop of the glass transition temperature in the presence of side chains is reported.[1] In particular, this effect strongly depends on the length of the side chains. In order to reveal the underlying microscopic mechanism, the relaxation dynamics of side-chain polymers was subject of many studies during the past few years.[1−8] Especially, the segmental relaxation of poly(*n*-alkyl methacrylate)s[1,2,9] or poly(α-*n*-alkyl *β*-L-asparate)s[6] was studied extensively as a function of the number of carbon atoms per side chain by means of broadband dielectric spectroscopy (BDS). Because of its wide frequency range, this method is well suited for exploring the temperature dependency of the relaxation processes and in particular for revealing the influence of the length of the side chain. However, since none of these polymers have a dipole moment oriented parallel to the backbone of the chain, there is only little knowledge about the influence of the length of the side chains on the end-to-end distance relaxation.

Appropriate polymers possessing a dipole moment parallel to the backbone of the chain are e.g. polyisoprene (PI) and poly(propylene oxide) (PPO). Because of this so-called type A dipole,[10] they display a dielectric normal mode, which is identified with the end-to-end relaxation of the polymer. Both PI and PPO were studied exhaustively by means of BDS.[11−19] It was found that the Rouse model was not able to describe the shape of the normal mode properly, which was attributed to the sample polydispersity.[12,20] Only recently, it has been reported that the Rouse model gives a reasonably good description of the shape of the normal mode relaxation of a low-M_w PI after incorporating the molecular weight distribution.[21] Yet, both PI and PPO are linear polymers, and hence no information about the influence of a side chain is gained by these experiments.

Lately, a systematic series of poly(alkylene oxide)s (PAO's) with up to 10 carbon atoms per side chain was synthesized.[22] Each of these PAO's possesses a type A dipole, and therefore the structural relaxation can be studied by BDS. In the past decade, also poly(butylene oxide) (PBO), which is a member of the familiy of the PAO's and differs from PPO by one additional carbon atom per side chain, was studied.[23−25] In these studies, shape as well as relaxation times of both normal and segmental mode are addressed, but only samples with low molecular weights[23,24] or with a rather large index of polydispersity[25] are used there. Only the recent synthesis of higher PAO's with high-M_w, all with a very narrow distribution of molecular weight,[22] for the first time allows for a detailed dielectric analysis of the influence of a long side chain on the end-to-end and segmental relaxation as well as on the glass transition temperature. Moreover, the dependency on the molar mass can be addressed. As will be shown by the present work, the glass transition temperature of these materials is well below room temperature. Therefore, normal mode and segmental relaxation can be observed over a wide temperature range without degrading the polymer.

The present work focuses mainly on the influence of the length of the side chain on the end-to-end distance (NM-) and segmental (α-) relaxation studied by BDS and rheology. Results of

*Corresponding author. E-mail: c.gerstl@fz-juelich.de and g.j.schneider@fz-juelich.de.

 Published on Web 05/10/2010

Table 1. Reaction Conditions and Polymer Characterization Results

	reaction conditions			characterization			
	reaction temp [K]	molar ratio of 18C6-KO*t*-Bu	$m_{toluene}/m_{monomer}$	reaction time [h]	M_n[a] [kg/mol]	M_w/M_n[b]	av deg of polymerization
PBO-10	253	1.5	1.0	39	10.2	1.04	140
PBO-50	253	3.0	1.0	188	50.6	1.06	700
PHO-10	258	0.75	1.0	70	9.4	1.03	95
POO-10	258	0.75	1.0	70	9.6	1.03	75
POO-50	259	3.0	1.0	187	48.9	1.05	380
PDO-10	288	1.0	1.8	96	9.3[c]	1.03	50

[a] From SEC coupled with triple detection. [b] From SEC, PS calibration. [c] From the signal intensities of the *tert*-butyl end groups and the terminal methyl groups of the monomer units.

both methods are analyzed with respect to the relaxation times and the temperature dependence of the latter and are compared to theoretical expectations. Because of the presence of the side chains, different molar masses refer to the same degree of polymerization. Therefore, also the contribution of the molar mass per backbone bond is addressed. Furthermore, the glass transition temperature is studied by means of differential scanning calorimetry. Finally, the structural relaxation observed by BDS is compared to the results of the rheological measurements.

Experiment

Polymer Synthesis and Characterization. All manipulations were carried out at a high-vacuum line or in a glovebox filled with argon (M Braun, Unilab). The water level in the glovebox was usually 1 ppm and the oxygen level below 0.1 ppm. The flasks for all manipulations were equipped with Teflon stopcocks that allowed transferring materials between vacuum line and glovebox without contamination with air. The purification of all materials as well as the monomers 1,2-butylene oxide, 1,2-hexylene oxide, and 1,2-octylene oxide is described in ref 22. 1,2-Dodecene oxide (Aldrich, 97%) was first distilled using an apparatus, which contained a 30 cm column equipped with an evacuated silver coated insulating jacket and filled with wire mesh rings (3500 mesh/cm^2) made of stainless steel (Normag). The distillation was carried out at a pressure of 17 mbar. The fraction distilling at 120.5−121 °C was used for further purification. For this purpose the monomer was degassed at the vacuum line and distilled over CaH_2. The mixture was stirred at room temperature for 7 days, and then the process was repeated. A third drying step over CaH_2 was carried out at 100 °C for 4 days. In between each purification step the monomer was degassed to pump off the produced hydrogen gas. Finally, the dried 1,2-dodecene oxide was distilled from CaH_2 into a storage flask using an all-glass apparatus, attached to the vacuum line via a Teflon stopcock. After distillation the flask containing the CaH_2 was sealed off. The storage flask was kept in a glovebox at room temperature.

The polymers were synthesized by polymerizing 1,2-alkylene oxides at low temperatures using potassium *tert*-butanolate (KO*t*-Bu) as initiator and 18-crown-6 (18C6) as activator. A detailed procedure is given in ref 22. The relevant reaction conditions for the polymers synthesized in the present work are summarized in Table 1. In all cases toluene was used as solvent. For poly(1,2-butylene oxide) (PBO), poly(1,2-hexylene oxide) (PHO), and poly(1,2-octylene oxide) (POO) the mass ratios of monomer to solvent were 1.0. In case of poly(1,2-dodecene oxide) (PDO) the polymerization had to be carried out in a more diluted solution and at higher temperature because of the low solubility of PDO in toluene at low temperatures. Despite these unfavorable reaction conditions, the molecular weight distribution was narrow (Table 1). The polymers except PDO were purified by dissolution in freshly distilled heptane followed by washing with deionized water. Then the heptane was removed, and the polymer was dried under high-vacuum conditions. PDO was purified by precipitation in methanol and subsequent freeze-drying.

Size exclusion chromatography (SEC) experiments for polymer characterization were carried out using a Waters 150-CV plus instrument together with five Styragel columns with a porosity range from 105 to 500 Å at 30 °C. For the signal detection a Viscotec model TDA 300 triple detector with a differential refractometer, a differential viscometer, and a right angle laser light scattering detector were used at 35 °C. The solvent was THF at a flow rate of 1 mL/min, which was degassed using a Viscotec model VE 7510 instrument. Molecular weights were calculated using the Viscotec TriSEC 3.0 GPC software. Molecular weight distributions M_w/M_n were calculated with the help of polystyrene (PS) calibration. NMR spectra were obtained on a Varian Inova 400 MHz. All samples were measured at 295 K in $CDCl_3$ with a 5 mm PFG AutoX DB Probe. In some cases molecular weights were calculated from the signal intensities of the *tert*-butyl end groups at about 1.05 ppm and the terminal methyl groups of the monomer units at about 0.9 ppm.

The tacticity of the polymers was not determined; however, the measured tacticity of a poly(propylene oxide) sample synthesized under similar conditions showed the polymer to be fully atactic.

Methods. *Differential Scanning Calorimetry*. The glass transition temperatures T_G and, where applicable, ranges of crystallization and melting were determined using a TA Instruments Q2000 calorimeter. Thereto, sealed aluminum pans were filled with 11−14 mg of polymer, and a heating rate of 20 K/min was applied.

Broadband Dielectric Spectroscopy. The dielectric measurements were performed in a frequency range of 10^{-1}−10^9 Hz employing two different experimental setups depending on the frequency range. Between 10^{-1} and 10^7 Hz, the measurements were conducted using a high-resolution Alpha dielectric analyzer by Novocontrol GmbH. For the frequency range of 10^6−10^9 Hz, an Agilent impedance analyzer HP4291B was used. In each case, isothermal frequency measurements were carried out between 200 and 420 K with a temperature stability better than 0.2 K. For both setups, the samples were prepared between two gold-plated electrodes of 20 and 10 mm diameter, respectively. Teflon spacers of 0.1 mm thickness and negligible area were applied to maintain the constant distance between the electrodes. All samples were stored in a vacuum oven at about 310 K before the measurement to lessen moisture and air entrapments as far as possible.

Rheology. Isothermal measurements were performed on a Rheometric Sci ARES rheometer equipped with a 2K FRT-N1 force rebalance transducer in a typical frequency range of 100−0.1 rad/s, using parallel plates with a diameter of 8 mm in view of the small amounts of sample. The temperature of the sample was controlled by a nitrogen flow oven with an accuracy better than ±1 K, and the temperature stability was better than ±0.5 K.

Data Evaluation and Theory. *Differential Scanning Calorimetry*. A glass transition appears as a step in a diagram where the (specific) heat flow is plotted versus the temperature, and the

glass transition temperature T_G corresponds to the point of inflection.[26] As crystallization temperature T_C the onset of crystallization is given. Since the melting of the samples occurred over a broad range, also the given melting temperature corresponds to the onset of melting, and additionally, the breadth of the melting range is specified.

Broadband Dielectric Spectroscopy. Usually, the Havriliak−Negami (HN) function[27]

$$\varepsilon^* = \varepsilon_\infty + \frac{\Delta\varepsilon}{(1+(i\omega\tau_{HN})^\beta)^\gamma} \quad (1)$$

is used to describe a dielectric relaxation process of a polymer. The exponents $0 < \beta, \gamma \leq 1$ denote the parameters characterizing the symmetric and asymmetric broadening of the maxima, respectively. In the present case, a sum of two HN functions and an additional conductivity term $\sim i\sigma/\omega^p$ was used, where $p \equiv 1$ for pure direct conductivity.[28,29]

The relaxation time corresponding to the maximum of the dielectric loss was calculated via

$$\tau_{max} = \tau_{HN}\left(\sin\frac{\beta\pi}{2(1+\gamma)}\right)^{-1/\beta}\left(\sin\frac{\beta\gamma\pi}{2(1+\gamma)}\right)^{1/\beta} \quad (2)$$

The temperature dependency of τ_{max} was then analyzed using the so-called Vogel−Fulcher equation[28]

$$\log\tau = \log\tau_\infty + \frac{A}{T-T_{VF}} \quad (3)$$

with a constant A, the extrapolated relaxation time at infinite temperature τ_∞, and the Vogel−Fulcher temperature T_{VF}.

The prediction of the Rouse model[30] for the dielectric loss of the normal mode is[31]

$$\frac{\varepsilon''(\omega)}{\Delta\varepsilon} = \frac{8}{\pi^2}\sum_{p:\mathrm{odd}}^{N}\frac{1}{p^2}\frac{\omega\tau_p}{1+\omega^2{\tau_p}^2} \quad (4)$$

Here, $\tau_p = \tau_R/p^2$ with the longest relaxation time called Rouse time

$$\tau_R = \frac{\zeta N^2 b^2}{3\pi^2 k_B T} \equiv \tau_{max,NM} \quad (5)$$

This is valid for a monodisperse, nonentangled linear polymer. For samples with higher molecular weight where entanglements are present, the longest relaxation time in the tube model is the disentanglement time

$$\tau_d = \frac{\zeta N^3 b^4}{\pi^2 k_B T d^2} \quad (6)$$

In eqs 5 and 6, ζ denotes the monomeric friction coefficient, N is the number of Kuhn segments with bond length b, and d is the tube diameter. Equation 6 neglects the speeding up of the dynamics by concurrent mechanisms like contour length fluctuations (CLF) and constraint release (CR).

Rheology. The single isothermal frequency sweeps of one sample were superimposed to master curves at a reference temperature $T = T_0$, using the well-known time−temperature superposition principle (TTS) (cf. e.g. Ferry's textbook[32]). The temperature dependency of the horizontal shift factors a_T can be described with the empirical Williams−Landel−Ferry (WLF) equation

$$\log a_T = -\frac{C_1(T-T_0)}{C_2+T-T_0} \quad (7)$$

which is equivalent to the Vogel−Fulcher equation (3). C_1 and C_2 depend on the polymer, the temperature of reference, and differ sometimes in the low-M_w range. The real and imaginary part, $G'(\omega)$ and $G''(\omega)$, of the complex modulus were fitted with different models, depending on the applicability. To the results of the low-M_w PBO and PHO, the prediction of the Rouse model[30]

$$G' = \frac{\rho RT}{M_w}\sum_{p=1}^{N}\frac{\omega^2{\tau_p}^2}{1+\omega^2{\tau_p}^2} \quad (8)$$

$$G'' = \frac{\rho RT}{M_w}\sum_{p=1}^{N}\frac{\omega\tau_p}{1+\omega^2{\tau_p}^2} \quad (9)$$

was fitted. For the high-M_w PBO, an implementation of the reptation model by Likhtman and McLeish[33] was used. There, a function $\mu(t)$ for the occupation of tube segments by a single chain reflecting CLF motion and reptation out of the tube, a term $R(t)$ describing CR via a Rouse-like motion of the tube itself, and expressions for the relaxation of longitudinal modes and the fast Rouse motion inside the tube are combined. This yields an expression for the relaxation modulus

$$G(t) = G_e\left(\frac{4}{5}\mu(t)R(t) + \frac{1}{5Z}\sum_{p=1}^{Z-1}\exp\left(-\frac{p^2 t}{\tau_R}\right) + \frac{1}{Z}\sum_{p=Z}^{N}\exp\left(-\frac{2p^2 t}{\tau_R}\right)\right) \quad (10)$$

with the entanglement modulus G_e, the number of entanglements per chain Z, and the number of Rouse beads N. Further details on the model can be found in the corresponding article.[33]

However, since some discrepancies and other definitions of M_e are reported , and as shown below, the measured moduli are rather low, the width of the plateau is judged to give a more accurate estimate for Z.[33,34]

Table 2. Crystallization T_C, Melting T_m, and Glass Transition Temperatures T_G Measured by DSC and Dielectric Glass Transition Temperatures $T_{G,\varepsilon}$ (All Values in K)

	T_C	T_M	approx breadth of melting range	$T_G \pm 1$	$T_{G,\varepsilon}$
PBO-10				203	199.6
PBO-50				204	200.2
PHO-10				205	200.8
POO-10	247	249	50		199.6
POO-50	246	247	50		198.7
PDO-10	290	295	50		199.8[a]

[a] Corresponding to the average value of the other $T_{G,\varepsilon}$'s. Cf. text.

Results and Discussion

Differential Scanning Calorimetry (DSC). All transition temperatures obtained by DSC are listed in Table 2; the dielectric glass transition temperature $T_{G,\varepsilon}$ will be discussed in the next section. While for PBO and PHO glass transitions were observed, POO and PDO crystallized. It was not possible to avoid the crystallization. Yet there were signatures of a glass transition around 205 K in the case of POO-10 and 207 K in the case of POO-50 in the semicrystalline state. These glass transitions were broader than those of PBO and PHO, the error being ±2 K. For PDO-10, no glass transition was observed.

One can see that changing the molecular weight has no influence on the glass transition temperature T_G of PBO within the experimental error. Assuming that T_G is not influenced by crystallization, this holds also for POO. Then

again, extension of the side chains seems to result in a very slight increase of the T_G's although this is not stringent.

For the PAO's with a side-chain length of at least six carbon atoms crystallization occurred. The crystallization temperature T_C and melting temperature T_M of POO are independent of molecular weight. For PDO-10, both T_C and T_M are significantly higher than for POO, whereas the breadth of the melting range is approximately the same.

The concept of the free volume predicts an increase of T_G with growing M_w up to a limiting value $T_{G,\infty}$ for infinite molecular weight. Also, packing effects that can be related with configurational entropy lead to similar tendencies for T_G. For low molecular weights T_G rises very fast and then bends rather quickly into a smaller slope, staying approximately constant from a sufficiently large M_w.[35,36] For example, at $M_w \approx 15$ and 10 kg/mol, the glass transition temperatures of polystyrene[37,38] and polypropylene[39,40] have practically reached their high-M_w limit. For polystyrene, Majeste et al.[41] report a critical entanglement molecular weight $M_c \approx 35$ kg/mol, which corresponds to an entanglement molecular weight M_e in the order of the M_w necessary for a constant T_G. Since the increase of T_G with M_w is in our case within the experimental error, we conclude that we do not observe the strong increase in T_G for very small M_w. The T_G's hence correspond approximately to the constant limiting values or are at least close to them.

For polymers having alkyl side chains it is considered a general phenomenon that T_G decreases markedly with increasing length of the side chain, e.g., for the poly(*n*-alkyl methacrylate)s (P*n*MA's) a significant descent of ~150 K from PMMA to P*n*DMA is observed. The absolute values of the respective T_G's thereby depend on the tacticity of the samples.[4,9,42] This effect is usually attributed to internal plasticization phenomena.[2,43,44] However, the almost constant T_G's reported in the present work are in sharp contrast to that. A possible reason for this might be a different interaction of the side chains with the main chain in the P*n*MA's than in the PAO's caused by the different chemical structure. While the alkyl side chains of the P*n*MA's are connected to the main chain via a carboxyl group there is no such connecting piece in the PAO's, and the latter do have an additional oxygen atom per monomeric unit in the main chain. This difference might result in a different interplay between main and side chain: the behavior of the glass transition of the main chain could be influenced more strongly by the dynamics of the side chains whose "glass transition" is commonly found to be below 200 K and rising slightly with increasing length of the side chains.[1,2] The combination of these opposing tendencies could lead to the observed behavior.

Only in the case of POO both T_G and T_C are observed, where $T_C/T_G = 1.16 \pm 0.01$. This differs from the empirical Beaman–Bayer rule $T_C \approx (3/2)T_G$,[45,46] which is valid for many polymers. If it is assumed that the PAO's are purely atactic as suggested by the tacticity of a poly(propylene oxide) sample (cf. the synthesis section Polymer Synthesis and Characterization), it has to be concluded that the crystallization is side-chain crystallization. This is a feature not uncommon for polymers with long alkyl side chains.[5,6] This may explain the above-mentioned deviation from the Beaman–Bayer rule as in this case crystallization and glass transition would result from different parts of the polymer and thus be independent. However, for energetic reasons, it might be favorable for the polymers with the longer side chains to assume a syndiotactic conformation. Then a main-chain crystallization would be possible. Hence, since up to now measurements of the tacticity are not performed, a crystallization of the main chain cannot be fully excluded. Because of the unchanged polymerization conditions, this is considered rather unlikely, though.

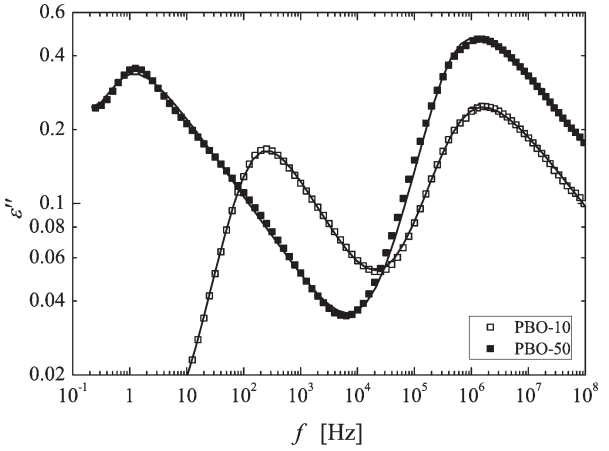

Figure 1. Dielectric loss $\varepsilon''(f)$ of PBO-10 and PBO-50 at 260 K. The lines correspond to the Havriliak–Negami fits.

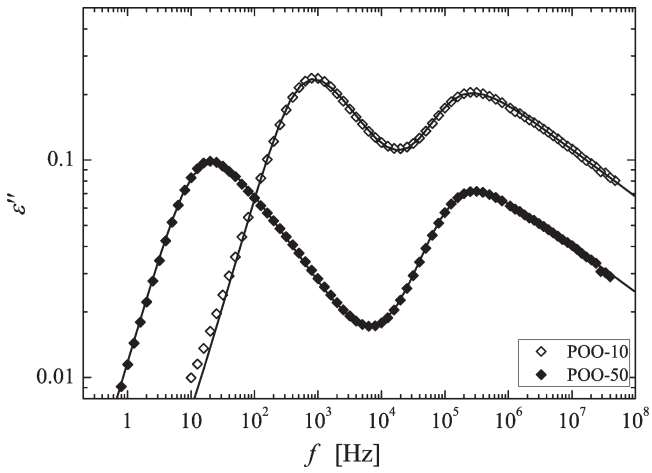

Figure 2. Dielectric loss $\varepsilon''(f)$ of POO-10 and POO-50 at 260 K. The lines correspond to the Havriliak–Negami fits.

The height of a T_G step is lower the smaller the amorphous fraction of the sample. Therefore, the fact that for PDO-10 no glass transition was visible might be due to a high degree of crystallinity. As stated above, quenching the sample in liquid nitrogen did not result in a suppression of the crystallization, either.

Broadband Dielectric Spectroscopy. Figures 1 and 2 show the dielectric loss ε'' vs frequency f of PBO and POO, respectively, each at low and high molecular weight. For clarity, error bars are omitted since all errors are within the symbol size. The lines correspond to fits with the Havriliak–Negami model as described in the Data Evaluation and Theory section. Since the depicted spectra were recorded during cooling, the POO samples were amorphous (cf. Table 2). Two peaks are clearly discernible: the peak at lower frequencies can be attributed to the normal mode relaxation, i.e., the relaxation of the end-to-end vector of the polymer chains. It is shifting to lower frequencies with increasing molecular weight for both PBO and POO. This is equal to a decrease in mobility with increasing molecular weight which is a typical feature of the normal mode relaxation. Contrarily, there is no molecular weight dependency for the peak at higher frequencies. Thus, it can be assigned to the segmental or α-relaxation of the polymer, which is only

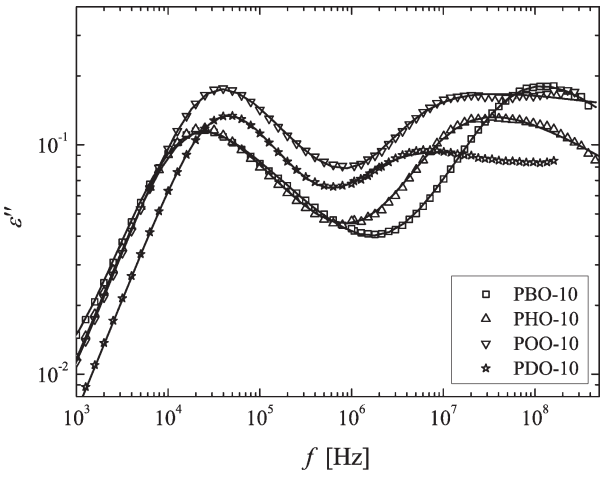

Figure 3. Dielectric loss $\varepsilon''(f)$ of PBO-10, PHO-10, POO-10, and PDO-10 at 310 K. The lines correspond to the Havriliak−Negami fits.

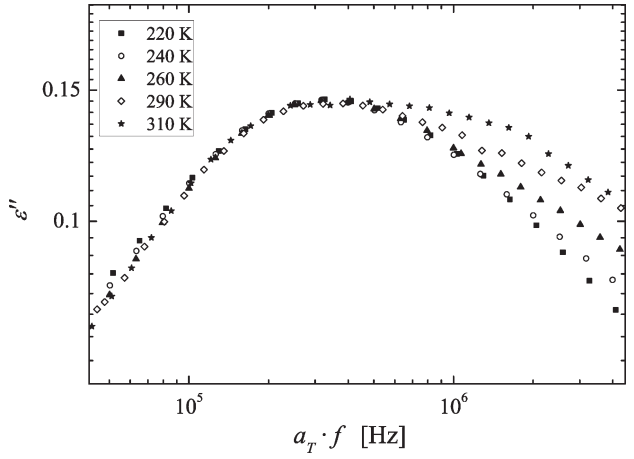

Figure 4. Master plot of the α-relaxation of PHO-10; curves were shifted to the peak position at 260 K.

dependent on the chemical structure of the respective segments.[28] These attributions will be further substantiated by the following discussion.

In Figure 3, a comparison of spectra of all low-M_w samples is shown. One can see that the normal mode relaxation is equally slow for PBO-10 and PHO-10 and fastest for PDO-10. For the α-relaxation, the effect is the opposite: the maximum dielectric loss of PBO-10 appears at higher frequencies than that of PHO-10, POO-10, and PDO-10.

A systematic broadening of the α-relaxation with increasing temperature was observed for PHO, POO, and PDO, i.e., the samples with the longer side chains. Exemplary for PHO-10, this is shown in Figure 4. There, a superposition of the α-peaks at different temperatures is given, where the reference temperature is 260 K. The effect is clearly visible, and for 310 K the relaxation process seems to exhibit a double-peak structure. For even higher temperatures the process already shifted out of the experimental window. Since this phenomenon only occurs when larger side groups are present, this might indicate a separate relaxation of the side chains. This process maybe corresponds to the so-called α_{PE} process which is observed for other polymers having alkyl side chains, e.g., for the P*n*MA's.[1] Since the side chain itself has no dipole moment, the presence of a separate side chain relaxation in the dielectric spectrum can be explained by considering that this motion also involves a small fluctuation of the dipolar unit. At higher temperatures the motions would be more decoupled (in time scale) from that of the main chain and would manifest as a slightly broader whole relaxation.

Table 3. Average Values of the Parameters for Symmetric and Asymmetric Broadening of Normal Mode and α-Relaxation

	$\overline{\beta_{NM}}$	$\overline{\gamma_{NM}}$	$\overline{\beta_\alpha}$	$\overline{\gamma_\alpha}$
PBO-10	1	0.42 ± 0.01	0.90 ± 0.07	0.39 ± 0.11
PBO-50	1	0.33 ± 0.01	0.96 ± 0.05	0.34 ± 0.08
PHO-10	1	0.54 ± 0.03	0.91 ± 0.06	—[a]
POO-10	1	0.58 ± 0.05	0.96 ± 0.03	—[a]
POO-50	1	0.43 ± 0.01	0.96 ± 0.06	—[a]
PDO-10	1	0.68 ± 0.02	0.91 ± 0.04	—[a]

[a] See text.

Wherever this broadening occurred, the slowest relaxation, i.e., the low-frequency part of the peak, is taken to be the α-relaxation. This choice is suggested by the way the peaks evolve with temperature.

In order to discuss the data, we applied the fitting procedure specified in the Theory section. This yielded a very good description of all spectra. The resulting shape parameters, except for γ_α of PHO, POO, and PDO, are independent of temperature within the error bars as long as the samples were amorphous. The corresponding mean values $\overline{\beta_{NM/\alpha}}$ and $\overline{\gamma_{NM/\alpha}}$ are listed in Table 3. No errror is given for $\overline{\beta_{NM}}$ since it is smaller than ±0.01 in all cases. For POO and PDO, all averages were calculated from the values obtained in the amorphous range. No $\overline{\gamma_\alpha}$ was calculated for PHO, POO, and PDO as they showed the above-mentioned systematic broadening with increasing temperature.

It can be observed that $\overline{\beta_{NM}}$ — the parameter for the symmetric broadening of the normal mode — is equal to 1 for all samples. Comparing $\overline{\gamma_{NM}}$ for the low-M_w samples shows that the values are greater for longer side chains. This means the asymmetric broadening becomes weaker with increasing length of the side chains. This is also valid for the high-M_w samples, but here the normal mode is in general broader than for the shorter chains. For the α-relaxation, $\overline{\beta_\alpha}$ is constant within the error bars for all samples. It does not change as the side group enlarges and is independent of molecular weight. Also, $\overline{\gamma_\alpha}$ of PBO shows no dependency on molecular weight.

The Rouse model prediction (cf. eq 4) results in Havriliak−Negami shape parameters $\beta_{NM} = 1$ and $\gamma_{NM} = 0.7$.[15] While the reported $\overline{\beta_{NM}}$ concur exactly with this theoretical value, the values obtained for $\overline{\gamma_{NM}}$ are all lower than the theoretical ones, except for $\overline{\gamma_{NM}}$ of PDO-10. From the data reported by Kyritsis et al.[24] for low-M_w PBO's (M_w = 970−4500 g/mol), we calculated $\gamma_{NM} \approx 0.7-0.65$; i.e., the asymmetric broadening increases slightly with M_w. The $\overline{\gamma_{NM}}$'s observed for PBO-10 and PBO-50 here follow this trend. This leads to the conclusion that the Rouse prediction is fulfilled only for polymers with a very low degree of polymerization. Imanishi et al.[12] reported equivalently that for polyisoprene (PI) the high frequency part of the dielectric loss is not described satisfactorily by the Rouse model but found no increase of the broadening for larger M_w's. A further discussion on this topic can be found at the end of this section.

It is a general finding that for higher molecular weights of linear polymers the degree of polymerization is not affecting the shape of the segmental relaxation.[47−49] The constant values for $\overline{\beta_\alpha}$ and $\overline{\gamma_\alpha}$ for PBO reported here are in agreement with this.

In Figures 5 and 6, the logarithm of the relaxation times $\tau_{max} = 1/(2\pi f_{max})$ of normal mode and α-relaxation, respectively, are plotted versus the inverse temperature (Arrhenius plot). In

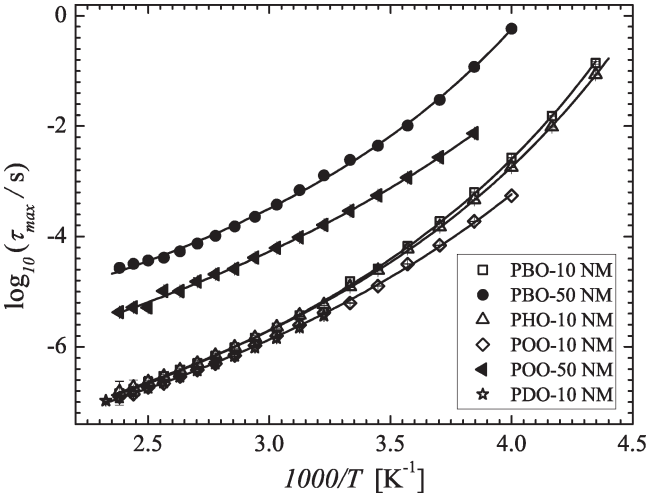

Figure 5. Relaxation times of the normal mode plotted vs the inverse temperature: empty symbols, results for M_w = 10 kg/mol; filled symbols, results for M_w = 50 kg/mol. The lines correspond to the Vogel−Fulcher fits.

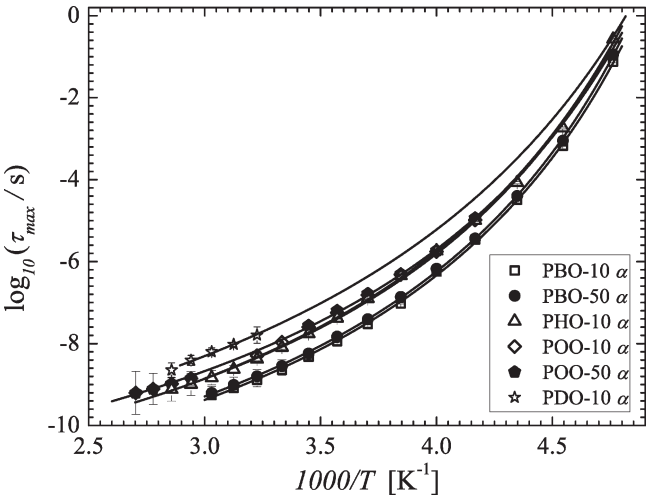

Figure 6. Relaxation times of the α-relaxation plotted vs the inverse temperature: empty symbols, results for M_w = 10 kg/mol; filled symbols, results for M_w = 50 kg/mol. The lines correspond to the Vogel−Fulcher fits; concerning the fit of PDO-10: see text.

each case, τ_{max} was calculated from the Havriliak−Negami relaxation times τ_{HN} using eq 2. Only values from the amorphous ranges of the samples are used. This leaves only very few data points for the α-relaxation of PDO-10, since for higher temperatures the process shifted out of the experimental window and for lower temperatures the sample crystallized.

The relaxation times of the normal mode depicted in Figure 5 strongly depend on the molecular weight. The relaxation is slowed down with increasing M_w, and at first glance, the samples with longer side chains for both high and low M_w seem to relax faster. The latter, however, is comprehensible when one has a look at the degrees of polymerization (cf. Table 1): as the side group of POO is larger than the one of PBO, POO has a lower degree of polymerization at the same molecular weight, and its backbone is therefore shorter and can thus relax faster. The different spacings between PBO-10 and PBO-50, on the one hand, and POO-10 and POO-50, on the other, can be explained as follows: The entanglement molecular weight M_e of poly(propylene oxide) (PPO) is given in the literature to be around 6 kg/mol.[50] 43/58

Table 4. Parameters of the Fits with the Vogel−Fulcher Equation

	$\log(\tau_\infty/s)$	A	T_{VF} [K]
	(a) Normal mode		
PBO-10 NM	−9.2 ± 0.1	630 ± 20	155 ± 2
PBO-50 NM	−6.9 ± 0.1	570 ± 30	164 ± 4
PHO-10 NM	−9.15 ± 0.03	622 ± 8	153 ± 1
POO-10 NM	−9.3 ± 0.1	650 ± 30	143 ± 4
POO-50 NM	−7.9 ± 0.2	720 ± 60	135 ± 8
PDO-10 NM	−9.02 ± 0.05	560 ± 20	153 ± 4
	(b) α-relaxation		
PBO-10α	−12.6 ± 0.1	550 ± 20	162 ± 2
PBO-50α	−12.5 ± 0.1	550 ± 20	162 ± 1
PHO-10α	−12.1 ± 0.1	560 ± 30	161 ± 2
POO-10α	−11.9 ± 0.2	560 ± 40	159 ± 5
POO-50α	−12.0 ± 0.1	590 ± 40	157 ± 4
PDO-10α[a]	−11.9 ± 0.3	640 ± 60	154 ± 4

[a] For the fitting procedure cf. text.

of the molecular weight of PPO is located in the polymer backbone; hence, the backbone of a PPO molecule with 6 kg/mol weighs ≈4.4 kg/mol. Assuming that the "entanglement backbone weight" $M_{e,bb}$ for the higher PAO's is approximately the same or a bit higher (which is likely due to the larger side group), it can be concluded that PBO-10 ($M_{w,bb}$ = 6090 g/mol) is on the threshold to the entanglement regime while PHO-10 ($M_{w,bb}$ = 4030 g/mol), POO-10 ($M_{w,bb}$ = 3215 g/mol), and PDO ($M_{w,bb}$ = 2185 g/mol) are too short to form entanglements. This assumption is supported, on the one hand, by the rheology data presented in the next section and, on the other, by the scaling of the relaxation times of low- and high-M_w samples:

$$\log \frac{\tau_{\text{low } M_w}}{\tau_{\text{high } M_w}} = x \log \frac{M_{w,\text{low}}}{M_{w,\text{high}}} \qquad (11)$$

Since the ratio of molar masses is independent of temperature, eq 11 requires that the ratio of the τ's will be independent of temperature, too. That this is the case can be seen in Figure 5. We found x = 3.2 for PBO and 2.2 for POO. The former value agrees well with eq 6, portending that both PBO samples are entangled. The latter value is very close to 2, indicating that even POO-50 shows Rouse-like behavior and hence is barely entangled. Consequently, the entanglement molecular weight of POO has to be much higher than for the samples with shorter side chains, which supports the statement that the presence of a larger side group "should strongly inhibit the reptation mechanism".[32]

The Arrhenius plot for the α-relaxation is shown in Figure 6. One observes that the relaxation times of PBO-10 and PBO-50 as well as the ones of POO-10 and POO-50 coincide and are therefore independent of molecular weight. This is in agreement with the results for PBO's of several molecular weights reported in the literature.[24,25] Furthermore, the relaxation times of the α-process increase systematically from PBO over PHO and POO to PDO. From that, one can conclude that the presence of a larger side group slows down the relaxation of the chain segments. Figure 6 also shows that the difference between the respective α-relaxation times increases with increasing temperature. This may be explained as follows: The ends of the side chains could act as plasticizers for the side-chain motion. With the end groups being farther and farther away from the dipolar group, this would result in a slower dipole motion for larger side chains. As T_G is approached, assuming an increasing collectivity of motion close to T_G, the motion of the dipolar

Table 5. Fragility of the PAO's

	m
PBO	77 ± 3
PHO	71 ± 3
POO	68 ± 5
PDO	60 ± 6

unit would involve more and more molecular groups, and the effect of the location of the end group then becomes less relevant.

The data depicted in Figures 5 and 6 were fitted with the empirical Vogel−Fulcher law (eq 3) which yields a good description. For the parameters of the normal mode relaxation (cf. Table 4a) the values differ for samples with the same length of the side chain and also for samples with the same molecular weight, although they are close together for the different low-M_w samples.

As expected, the obtained parameters for the α-relaxation (Table 4b) of the high- and low-M_w samples of both PBO and POO are the same within the fitting error. For PHO-10, the Vogel−Fulcher parameters of the α-relaxation are in the same range as for the other samples. Since for PDO-10 only a few points are available, the fitting was performed using the following procedure: the temperature where $\log(\tau_{\max,\alpha}/\mathrm{s}) = 2$ was taken as a "dielectric glass transition temperature", $T_{G,\varepsilon}$, and the VF fits of the other samples were extrapolated to this point. Then the mean value of these $T_{G,\varepsilon}$'s given in Table 2 was calculated and used as an additional data point for the fitting of the α-relaxation of PDO-10. The parameters given in Table 4b correspond to the thus-obtained values.

The $T_{G,\varepsilon}$'s are all a bit lower than the calorimetric glass transition temperatures. However, the $T_{G,\varepsilon}$'s of PBO-10, PBO-50, and PHO-10 do have the same relations as in the calorimetric case. For both POO samples, $T_{G,\varepsilon}$ is almost the same as for PBO-10, and hence lower than T_G, indicating that the glass transition in the completely amorphous state may differ from the one in the semicrystalline state.

In contrast to the findings of Yamane et al.[25] for PBO, the parameters A and T_{VF} for normal and segmental mode of one sample are in general not equal. Additionally, the fragility or steepness index[51,52]

$$m = \left.\frac{\mathrm{d}\log\tau_{\max,\alpha}}{\mathrm{d}\frac{T_\tau}{T}}\right|_{T=T_\tau} \tag{12}$$

with $T_\tau = T(\tau = 10^2\ \mathrm{s})$ of the different PAO's was calculated. Since the α-relaxation and the glass transition temperatures do not depend significantly on M_w, the values for the same polymer with different M_w are equal within the error bars. Therefore, the results compiled in Table 5 are mean values where more than one M_w was available. The fragility of PBO agrees with the 78 ± 1 given in ref 23. One observes a decrease of m with increasing length of the side chains. This is in accordance with the results for the P*n*MA's, where a corresponding trend is reported.[42,44] This means that the fragilities of the PAO's and the P*n*MA's evolve in the same way with increasing length of the side chains despite the different behavior of the glass transition temperatures.

It is known that the prediction of the Rouse model[30] for the dielectric loss of the normal mode (eq 4) does not give an exact description of the experimental results.[12,20,21,53] Also, the data presented here show a stronger asymmetric broadening than expected as was already stated above. Imanishi et al.[12] attributed the deviations on the high-frequency side of ε'' of their PI samples partly to the polydispersity and partly to a wedge-shaped distribution of relaxation times. Riedel et al.[21] found a very good agreement of their data with the Rouse model after including a distribution of molecular weight and ascribe the remaining deviations to the nonperfect microstructure of the PI samples.

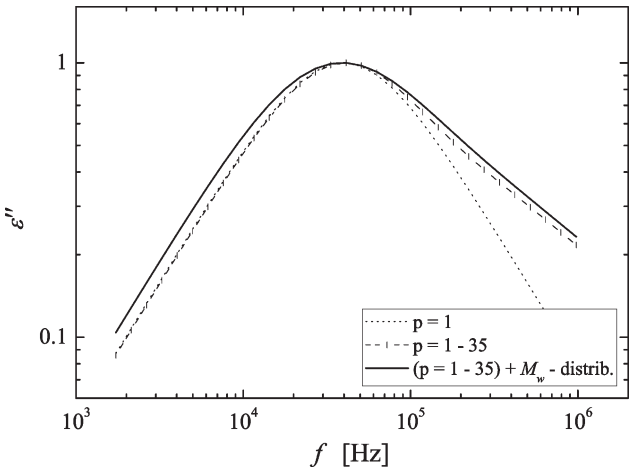

Figure 7. Calculated normal mode relaxation for the first Rouse mode only, for Rouse modes 1−35, and for Rouse modes 1−35 plus a distribution of molecular weight.

To illustrate the effect of a distribution of molecular weights, Figure 7 shows the difference in the calculated dielectric loss between the inclusion of the first Rouse mode only, the Rouse modes 1−35, and the inclusion of a M_w distribution to the latter. For this visualization we used a Poisson-shaped distribution with an arbitrary index of polydispersity of 1.15. It can be seen that the relaxation of the first Rouse mode is equal to a Debye relaxation with slopes of 1 and −1 on the low- and high-frequency wing, respectively. An asymmetric broadening arises from the inclusion of higher Rouse modes. Summing up to even higher modes takes effect only at even higher frequencies and therefore does not affect the slopes visibly. Additionally including a distribution of molecular weight leads to a broadening of the maximum and therefore to a rising of both low- and high-frequency wing of the dielectric loss, but without changing the slopes.

For the comparison with the experimental data we followed a similar procedure as Riedel et al.:[21] The α-relaxation was calculated using the Havriliak−Negami parameters obtained before, and instead of using a Gaussian M_w distribution, we extracted a function $G(M,M_n)$ directly from the SEC traces of the samples, where M_n is the molecular weight of the sample as it is given in Table 1. 35 modes were included in the calculation, and τ_1 was taken to be related to the peak position of the normal mode via $\tau_1 = (2\pi f_{\max})^{-1}$. We then calculated the dielectric normal mode of the low-M_w samples via multiplying eq 4 by $G(M,M_n)$ and substituting τ_p by

$$\tau_p(M) = \tau_p(M_n)\left(\frac{M}{M_n}\right)^2 \tag{13}$$

In Figure 8 as an example the comparison of the measured spectrum of PBO-10 at 260 K is shown together with the corresponding calculation. The dotted line describing the α-relaxation is obtained by the Havriliak−Negami fit. One can see that the low-frequency part of the normal mode peak is described almost perfectly, whereas there is a considerable

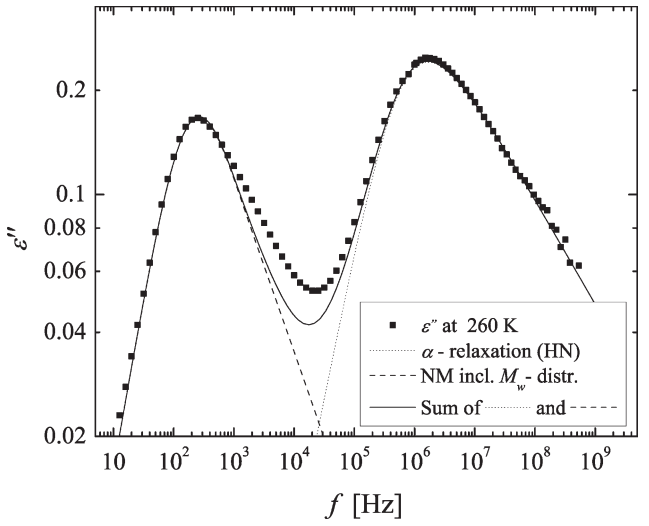

Figure 8. Measured dielectric loss $\varepsilon''(f)$ of PBO-10 at 260 K and calculated normal mode relaxation.

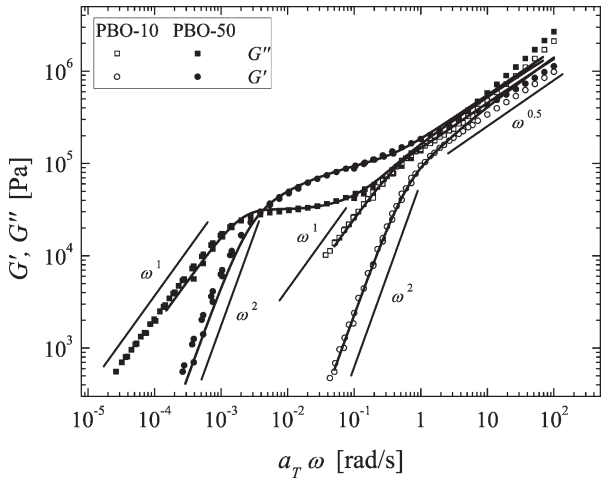

Figure 9. Storage modulus G' and loss modulus G'' of PBO-10 (open symbols) and PBO-50 (closed symbols). The reference temperature is 223 K. The lines correspond to the fits with the Rouse model (for PBO-10) and Likhtman's model (for PBO-50).

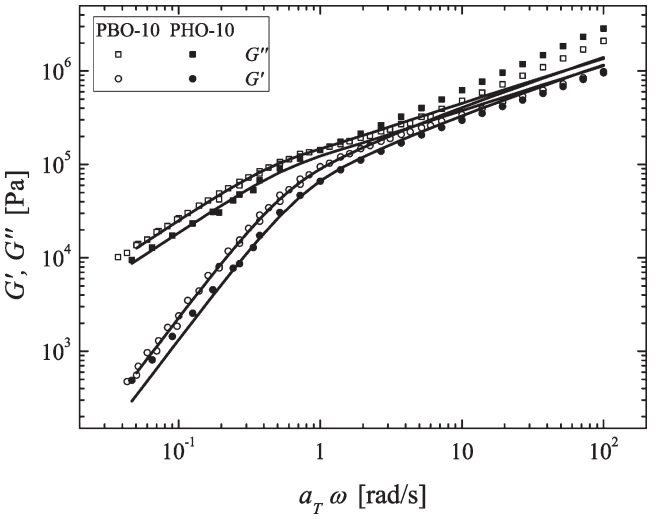

Figure 10. Storage modulus G' and loss modulus G'' of PBO-10 (open symbols) and PHO-10 (closed symbols). The reference temperature is 223 K. The lines correspond to fits with the Rouse model.

difference between the data points and the calculated values in the high-frequency wing. The deviations start at frequencies only slightly above f_{max} and significantly below the frequency corresponding to the second dielectrically active Rouse mode ($p = 3$). It is not possible to explain this by assuming that with a certain probability the side chain is attached to the first carbon atom of the monomer instead of to the second one which would lead to a reduction of the dipole moment of the chain. In such a case, also at the low-frequency side discrepancies would have to be visible, especially for the higher molecular weights where the majority of the polymers would have some misplacements of that sort. This is not observed for any of our samples. Another explanation one could think of is a dipole inversion of a sort such that one polymer chain has two (or more) resulting dipole moments in opposite directions. This, however, is with the used synthesis method chemically not possible. Using an exponent greater than 2 in eq 13 in view of the possible presence of entanglements leads to a distinctly broader peak than experimentally observed, while the high-frequency wing is still underestimated. The discrepancies between experiment and calculation thus seem to indicate deficiencies of the Rouse model in describing the proper mode spectrum for poylmers with larger side groups.

Rheology. For PBO-10, PBO-50, and PHO-10, master curves for the real and imaginary part of the complex shear modulus $G^*(\omega)$ at a reference temperature $T_0 = 223$ K were obtained and are shown in Figures 9 and 10. The corresponding WLF parameters are summarized in Table 6. In the case of PBO (Figure 9), simple visual inspection of the ω-dependence already indicates that the two molecular weights belong to the unentangled and (moderately) entangled region, judging from the absence and presence of a more or less pronounced plateau region in the storage modulus G', respectively. The comparison between PBO-10 and PHO-10, on the other hand, is shown in Figure 10. The curves of both samples agree well with the simple Rouse model for unentangeld polymers. For both samples the expected signatures for simple, monodisperse linear polymers are received: In the terminal regime the slopes are constant with values of 1 and 2 for loss and storage molulus. Near the region of the dynamic glass transition, the slopes of G' and G'' are as usual equal or close to 0.5 as predicted by the Rouse model. The solid curves in Figures 9 and 10 are either fits to the Rouse model or the present most molecularly based approach following Likhtman and McLeish.[33]

Table 6. WLF Parameters[a]

	C_1	C_2 [K]
PBO-10 ($T_0 = 223$ K)	7.5	48
PBO-50 ($T_0 = 223$ K)	9.4	58.1
PBO-50 ($T_0 = 243$ K)	7.6	93
PHO-10 ($T_0 = 223$ K)	7.17	37.98

[a] The average error is below 0.2 for C_1 and below 2.5 K for C_2.

Fits of the Rouse model (cf. Data Evaluation and Theory section) to the unentangled species lead to the Rouse time τ_R and prefactors depending on the size of the chain. For PBO-10 and PHO-10, the amplitudes were virtually identical with 0.11 MPa and the τ_R's were 1.39 and 1.07 s, respectively.

The most interesting polymer in this context is PBO-50 since it is the only entangled one and will be able to prove the consistency. The data at $T_0 = 243$ K were fitted with the full tube model, taking into account contour length fluctuations to the reptation as well as constraint release due to local tube Rouse motion. The parameters still depend a bit on the

assumption for the constraint release parameter c_ν which is related to the relative hop distance in terms of tube diameters. The number of entanglements varies between 5.5 and 6 for $c_\nu = 0$ and 0.1, respectively. The entanglement time τ_e is unaffected by the choice of c_ν and is 0.012 s at $T_0 = 243$ K, which can be rescaled to a reference temperature of 223 K resulting in $\tau_e = 1.55 \pm 0.3$ using Table 6 and error bars on the WLF constants.

For the Rouse time, the relation $\tau_R = \tau_e Z^2$ holds. Since τ_e obtained from the fit of PBO-50 is approximately equal to the Rouse time of PBO-10, this proves that the molecular weight of PBO-10 is smaller than or fairly equal to the molecular weight between entanglements M_e. The times correspond to an average number of entanglements $Z \approx 0.9 \pm 0.1$, which is nearly 1, and so in a good approximation $M_e = M_w/Z = 10\,700 \pm 1500$ g/mol. This is consistent with $M_e \approx 8800 \pm 1100$ g/mol, calculated using Z(PBO-50). Extrapolations for the other PAO's cannot be made due to the lack of reliable τ_e values.

However, estimates for M_e can be obtained in a different way: Similar to the noticed predictability of chain parameters from both experimental and simulation work for poly(olefine)s,[54,55] basing solely on the mass per backbone bond m_b, a workable hypothesis can be framed. Since the PAO's may be regarded as substituted PEO chains, we introduced the relationship

$$\frac{\langle R^2\rangle_0}{M} = \frac{m_{0,\mathrm{PEO}}}{3m_b}\left(\frac{\langle R^2\rangle_0}{M}\right)_{\mathrm{PEO}} = \frac{44}{3m_b}\left(\frac{\langle R^2\rangle_0}{M}\right)_{\mathrm{PEO}} \quad (14)$$

in analogy to the relation for poly(ethylene) and higher poly(olefine)s in ref 54. $(\langle R^2\rangle_0/M)_{\mathrm{PEO}}$ was determined and confirmed earlier to be 0.805 Å^2 mol/g.[55]

For the PAO's, the mass per backbone bond is m_b(PPO) = 19.3, m_b(PBO) = 24, m_b(PHO) = 33.33, and m_b(POO) = 42.67 g/mol. Inserting the m_b's into eq 14 leads to $(\langle R^2\rangle_0/M)$ for the PAO's in the above order: 0.61, 0.49, 0.35, and 0.28 Å^2 mol/g. Experimental chain dimensions are only known for PBO from θ-solution work ($\langle R^2\rangle_0/M = 0.49$ Å^2 mol/g)[56] and for POO (0.29 ± 0.01 Å^2 mol/g).[57] Both experimental values are in perfect agreement with our prediction. The packing length[58] is defined as

$$p = \frac{M}{\langle R^2\rangle_0 \rho N_A} \quad (15)$$

We took the density of PEO, ρ(PEO) = 1.06 g/cm^3, from ref 55 and measured ρ(PPO) = 1.01 g/cm^3, ρ(PBO) = 0.98 g/cm^3, ρ(PHO) = 0.94 g/cm^3, and ρ(POO) = 0.92 g/cm^3. With this, the values resulting for the packing lengths are 1.95 (PEO), 2.69 (PPO), 3.46 (PBO), 5.05 (PHO), and 6.45 (POO). Within the framework of the packing model it is assumed that p scales with the tube diameter d_t:

$$d_t \cong 19p \quad (16)$$

and therefore M_e can be expressed as

$$M_e = \frac{(19p)^2 M}{\langle R^2\rangle_0} \quad (17)$$

We obtain $M_e \approx 8800$, 26 000, and 53 500 g/mol for PBO, PHO, and POO, respectively. The value for PBO concurs perfectly with the above-mentioned M_e values resulting from the fits to the data. The high M_e resulting for POO within this estimate seems also reasonable since the relaxation times of the dielectric normal mode points at a not or only slightly entangled POO-50.

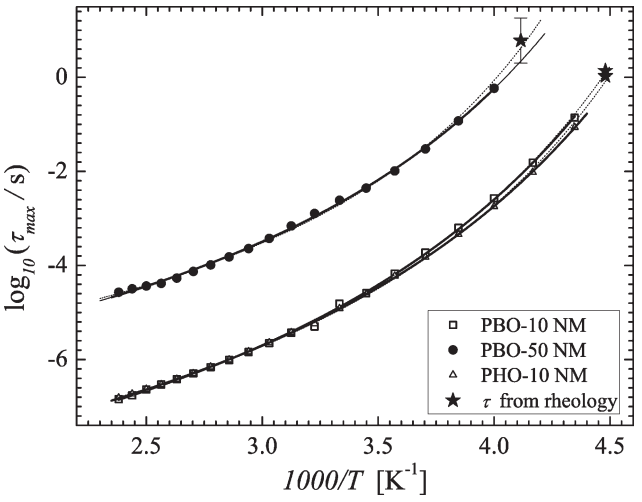

Figure 11. Relaxation times of the normal mode of PBO and PHO plotted versus the inverse temperature including the longest relaxation time obtained from the rheology measurements. The solid lines correspond to the (extrapolated) Vogel−Fulcher fits of the dielectric data; the dotted lines also include the rheology data.

Using these values for M_e, the plateau modulus $G_e = \rho RT/M_e$ at ambient temperature differs by as much as a factor of 6.25 going from PBO (0.25 MPa) to POO (0.04 MPa)! The value for G_e resulting from the fitting of PBO-50 with the tube approach is 0.15 MPa, being lower than the estimate, even if one considers the temperature dependence of the density. This may be due to microscopic air bubbles caused by the difficult preparation of the samples between the rheometer plates. Considering the latter and the fact that the estimated G_e is based on simple assumptions, the agreement is very good, though.

For all calculations in the above paragraph, we have ignored steric hindrance effects and, mostly, also temperature dependencies. The results are, however, physically sound in order to guide a further systhesis of the PAO's with respect to the interesting molecular weight where entanglements are formed. At the same time, we have to revisit the former observations that the glass transition temperature is constant for the different side-chain lengths: Because of the presumably very high M_e of POO, the limiting value of the glass transition temperature may still be some K above the ones given in the DSC-section. This would then result in an increase of T_G with increasing length of the side chains. An effective decrease of T_G as it is found for the P*n*MA's can be excluded for the PAO's.

Comparison of the Different Methods. In Figure 11, the Arrhenius plots of the normal mode relaxation of PBO-10, PBO-50, and PHO-10 are shown together with the corresponding relaxation times obtained from the fits to the rheology data. In case of PBO-50, this is the disentanglement time τ_d resulting from Likhtman's model, and in the case of the low-M_w samples it is the Rouse time τ_R. The Vogel−Fulcher fits to the Arrhenius curves were repeated considering also these additional data points. It turns out that for PBO-10 and PHO-10 there is almost no change in the fitting parameters compared to those obtained only from the dielectric data. For PBO-50, the value obtained from rheology is, within the error bars, consistent with the extrapolation of the fit of the dielectric data. The new fit, however, also gives a satisfying approximation of the dielectric data. We thus conclude that despite the fact that dielectric spectroscopy and rheology measure retardation and

relaxation, respectively, and although they probe microscopic properties on the one hand and macroscopic ones on the other, the respective longest relaxation times agree with each other.

Summary

We presented the results of differential scanning calorimetry, dielectric spectroscopy, and rheology experiments on different poly(alkylene oxide)s with two different molecular weights. For the samples with the longest side chains, crystallization occurred. The glass transition temperatures are almost independent of the molar mass and vary only slightly with the length of the side chains. This is also reflected by the relaxation times of the dielectric α-relaxation which depends scarcely on the molecular weight but slows down a little with the number of carbon atoms per side group. Additionally, the dielectric α-peak of the samples with side chains of at least four carbon atoms show a shoulder at high frequencies possessing a temperature-dependent shape. Perhaps this is an indication of a separate relaxation process of the side chains. The shape of the normal mode relaxation changes slightly with the molar mass and the length of the side chain. The corresponding relaxation times show a distinct dependency on both molar mass and side-chain length since the latter clearly influences the entanglement molecular weight M_e. A calculation based on the Rouse model incorporating an additional molar mass distribution was performed in order to theoretically describe the dielectric normal mode. However, we did not succeed in obtaining an accurate result.

For PBO and PHO, rheological experiments yielded results which are in accordance with the dielectric data. An estimate of M_e based on the number of entanglements on the one hand and the packing model on the other substantiated the values already suggested by the BDS results. This clearly demonstrates that M_e increases markedly with increasing length of the side group, being around 54 kg/mol for POO. A comparison of estimated chain dimensions with literature data for PBO and POO showed excellent agreement.

Acknowledgment. The present work has been carried out in the frame of the Joint Programme of Activities of the SoftComp Network of Excellence (Contract NMP3-VT-2004-502235) granted under the FP6 by the European Commission. C.G. acknowledges financial support by the International Helmholtz Research School of Biophysics and Soft Matter (IHRS BioSoft). A.A. and J.C. acknowledge the financial support provided by the Donostia International Physics Center (DIPC), the Basque Country Government (Ref. IT-436-07, Depto. Educación, Universidades e Investigación), and the Spanish Ministry of Science and Innovation (Grant MAT 2007-63681).

References and Notes

(1) Beiner, M.; Huth, H. *Nat. Mater.* **2003**, *2*, 595.
(2) Beiner, M. *Macromol. Rapid Commun.* **2001**, *22*, 869.
(3) Arbe, A.; Genix, A.-C.; Colmenero, J.; Richter, D.; Fouquet, P. *Soft Matter* **2008**, *4*, 1792.
(4) Hiller, S.; Pascui, O.; Budde, H.; Kabisch, O.; Reichert, D.; Beiner, M. *New J. Phys.* **2004**, *10*, 10.
(5) Out, G. J. J.; Turetskii, A. A.; Möller, M.; Oelfin, D. *Macromolecules* **1994**, *27*, 3310.
(6) Laredo, E.; Grimau, M.; Bello, A.; López-Carrasquero, F. *J. Non-Cryst. Solids* **2007**, *353*, 4324.
(7) del Val, J.; Alegría, A.; Colmenero, J.; Mijangos, C.; Martínez, G.; Millán, J. *Makromol. Chem.* **1989**, *190*, 3257.
(8) McCrum, N. G.; Read, B. E.; Williams, G. *Anelastic and Dielectric Effects in Polymeric Solids*; Dover Publications: New York, 1991; Reprint; primary publication: John Wiley & Sons Ltd.: London, 1967.
(9) Garwe, F.; Schönhals, A.; Lockwenz, H.; Beiner, M.; Schröter, K.; Donth, E. *Macromolecules* **1996**, *29*, 247.
(10) Stockmayer, W. H. *Pure Appl. Chem.* **1967**, *15*, 539.
(11) Adachi, K.; Kotaka, T. *Macromolecules* **1985**, *18*, 466.
(12) Imanishi, Y.; Adachi, K.; Kotaka, T. *J. Chem. Phys.* **1988**, *89*, 7593.
(13) Imanishi, Y.; Adachi, K.; Kotaka, T. *J. Chem. Phys.* **1988**, *89*, 7585.
(14) Boese, D.; Kremer, F. *Macromolecules* **1990**, *23*, 829.
(15) Schönhals, A. *Macromolecules* **1993**, *26*, 1309.
(16) Baur, M. E.; Stockmayer, W. H. *J. Chem. Phys.* **1965**, *43*, 4319.
(17) Ngai, K. L.; Schönhals, A.; Schlosser, E. *Macromolecules* **1992**, *25*, 4915.
(18) Schlosser, E.; Schönhals, A. *Colloid Polym. Sci.* **1993**, *91*, 158.
(19) Hayakawa, T.; Adachi, K. *Polymer* **2001**, *42*, 1725.
(20) Watanabe, H. *Macromol. Rapid Commun.* **2001**, *22*, 127.
(21) Riedel, C.; Alegría, Á.; Tordjeman, P.; Colmenero, J. *Macromolecules* **2009**, *42*, 8492.
(22) Allgaier, J.; Willbold, S.; Chang, T. *Macromolecules* **2007**, *40*, 518.
(23) Casalini, R.; Roland, C. M. *Macromolecules* **2005**, *38*, 1779.
(24) Kyritsis, A.; Pissis, P.; Mai, S.-M.; Booth, C. *Macromolecules* **2000**, *33*, 4581.
(25) Yamane, M.; Hirose, Y.; Adachi, K. *Macromolecules* **2005**, *38*, 9210.
(26) Wunderlich, B. *Thermal Analysis of Polymeric Materials*; Springer-Verlag: Berlin, 2005.
(27) Havriliak, S.; Negami, S. *J. Polym. Sci., Part C* **1966**, *14*, 99.
(28) Kremer, F.; Schönhals, A. *Broadband Dielectric Spectroscopy*; Springer-Verlag: Berlin, 2003.
(29) Riande, E.; Diaz-Calleja, R. *Electrical Properties of Polymers*; CRC Press: Boca Raton, FL, 2004.
(30) Rouse, P. E. *J. Chem. Phys.* **1953**, *21*, 1272.
(31) Adachi, K.; Wada, T.; Kawamoto, T.; Kotaka, T. *Macromolecules* **1995**, *28*, 3588.
(32) Ferry, J. D. *Viscoelastic Properties of Polymers*, 3rd ed.; John Wiley & Sons: New York, 1980.
(33) Likhtman, A. E.; McLeish, T. C. B. *Macromolecules* **2002**, *35*, 6332.
(34) Larson, R. G.; Sridhar, T.; Leal, L. G.; McKinley, G. H.; Likhtman, A. E.; McLeish, T. C. B. *J. Rheol.* **2003**, *47*, 809.
(35) Fox, T. C.; Flory, P. J. *J. Appl. Phys.* **1950**, *21*, 581.
(36) Montserrat, S.; Colomer, P. *Polym. Bull.* **1984**, *12*, 173.
(37) Ellison, C. J.; Mundra, M. K.; Torkelson, J. M. *Macromolecules* **2005**, *38*, 1767.
(38) Ueberreiter, K.; Kanig, G. *J. Colloid Sci.* **1952**, *7*, 569.
(39) Ke, B. *Polym. Lett.* **1963**, *1*, 167.
(40) Cowie, J. M. G. *Eur. Polym. J.* **1973**, *9*, 1041.
(41) Majeste, J.-C.; Montfort, J.-P.; Allal, A.; Marin, G. *Rheol. Acta* **1998**, *37*, 486.
(42) Beiner, M.; Huth, H.; Schröter, K. *J. Non-Cryst. Solids* **2001**, *279*, 126.
(43) Heijboer, J. Mechanical Properties and Molecular Structure of Organic Polymers. *Physics of Non-Crystalline Solids*; Elsevier: Amsterdam, 1965.
(44) Floudas, G.; Placke, P.; Štěpánek, P.; Brown, W.; Fytas, G.; Ngai, K. L. *Macromolecules* **1995**, *28*, 6799.
(45) Lechner, M. D.; Gehrke, K.; Nordmeier, E. H. *Makromolekulare Chemie*, 3rd ed.; Birkhäuser Verlag: Basel, 2003.
(46) Elias, H.-G. *Makromoleküle*, 6th ed.; Wiley-VCH: Weinheim, 1999.
(47) Runt, J. P.; Fitzgerald, J. J. *Dielectric Spectroscopy of Polymeric Materials − Fundamentals and Applications*; American Chemical Society: Washington, DC, 1997.
(48) Santangelo, P. G.; Roland, C. M. *Macromolecules* **1998**, *31*, 4581.
(49) Roland, C.; Ngai, K. L. *Macromolecules* **1996**, *29*, 5747.
(50) Mijovic, J.; Sun, M.; Han, Y. *Macromolecules* **2002**, *35*, 6417.
(51) Angell, C. A.; Sichina, W. *Ann. N.Y. Acad. Sci.* **1976**, *279*, 53.
(52) Böhmer, R.; Ngai, K. L.; Angell, C. A.; Plazek, D. J. *J. Chem. Phys.* **1993**, *99*, 4201.
(53) Doxastakis, M.; Theodorou, D. N.; Fytas, G.; Kremer, F.; Faller, R.; Müller-Plathe, F.; Hadjichristidis, N. *J. Chem. Phys.* **2003**, *119*, 6883.
(54) Fetters, L. J.; Lohse, D. J.; García-Franco, C. A.; Brant, P.; Richter, D. *Macromolecules* **2002**, *35*, 10096.
(55) Fetters, L. J.; Lohse, D. J.; Colby, R. H. Chain Dimensions and Entanglement Spacings. *Physical Properties of Polymers Handbook*; 2nd ed.; Mark, J. E., Ed.; Springer: New York, 2007.
(56) Matsushima, M.; Fukatsu, M.; Kurata, M. *Bull. Chem. Soc. Jpn.* **1968**, *41*, 2570.
(57) Hamley, I. W.; O'Driscoll, B. M. D.; Lotze, G.; Moulton, C.; Allgaier, J.; Frielinghaus, H. *Macromol. Rapid Commun.* **2009**, *30*, 2141.
(58) Fetters, L. J.; Lohse, D. J.; Richter, D.; Witten, T. A.; Zirkel, A. *Macromolecules* **1994**, *27*, 4639.